Impingement of Single Droplets on a Dry Smooth Surface at High Weber Numbers

B.W. Brinkmann* and T.J. Möller
Institut für Strömungsmechanik
Technische Universität Braunschweig
38106 Braunschweig Germany

Abstract

The vertical impingement of single water droplets on a smooth dry surface was experimentally investigated. A glass substrate was mounted on a rotating flywheel in order to obtain high impact velocities and high Weber numbers, respectively. Two different Weber numbers were observed by means of shadowgraphy technique: $\mathrm{We} = 5,000$ and $\mathrm{We} = 10,000$. The outcome of the measurement was analysed by digital image processing to quantify the distribution of the diameter of the resulting secondary droplets. This distribution of the droplet diameter is influenced by the Weber number and time during the impingement process. In addition, the verification was done that the camera system can largely resolve the secondary droplets, emerging during splashing impact. Aim of this investigation is to enable the evaluation of the total deposited mass after impingement. It is shown that the contribution of a high number of small droplets to the total secondary mass is little.

Introduction

The process of the impingement of droplets on solid surfaces is important for a wide range of technical applications like internal combustion engines, cooling, surface coating and ink jet printing. Since this process was first reported in [1] it has been presented in many further studies [2, 3, 4, 5]. Several reviews examine the impact of droplets on solid surfaces either dry or wetted. The different effects like bouncing, spreading and splashing occurring during the impact of a single droplet on solid and on liquid surfaces respectively are discussed by [6] and [7]. The dimensionless parameter used to quantify the impact energy of the droplet is the Weber number which identifies the ratio of impact inertia to surface force,

$$\mathrm{We} = \frac{\rho v^2 d_\mathrm{D}}{\sigma} \ , \tag{1}$$

where ρ is the liquid density, v the impact velocity, d_D the droplet diameter and σ the liquid surface tension. Further parameters influencing the outcome of the impingement on solid surfaces are the surface roughness and the wettability of the surface.

In [8] the impact on rough surfaces is discussed. But the authors also deal with the impact on a thin liquid film at $\mathrm{Re} = 3739$ and $\mathrm{We} = 354$ where they noticed two different sizes of secondary droplets in the beginning of the impact and $1 \cdot 10^{-3}$ s later: They assume the small secondary droplets to be ejected from the top of the crown in the beginning and the larger ones to be generated $1 \cdot 10^{-3}$ s later by the formation and disintegration of a torus containing the rest of the crown's edge.

For another class of processes with technical relevance like the soiling of ground vehicles and the icing of aircraft, respectively [9, 10, 11], the impact velocity and hence the corresponding Weber number is much higher. Only little work has been published covering this kind of the impingement process under high Weber number regime. The authors of [12] investigate the high-speed impact of small water droplets on a solid surface. The fingering phenomenon which occurs after the impact of a single droplet on a solid surface is observed for different Weber numbers and different surface roughness. In a further investigation [13] the same authors present a mathematical model based on the linear Rayleigh-Taylor instability to determine the wavelength of the perturbation around the impinging droplet. It is suggested the fingers separate from the surface for high Weber numbers. The impact of droplets on liquid layers with high Weber numbers is discussed in [14]. A regime diagram based on the variation of the Weber number is derived from the experimental results.

In the present study the impinging process of a single droplet on a solid dry surface is observed and analysed for Weber numbers up to $\mathrm{We} = 10,000$. The distribution of the resulting secondary droplets is determined by means of high speed photography and digital image processing.

*Corresponding author: benjamin.brinkmann@tu-braunschweig.de

Materials and Methods

According to [15] a moving droplet disintegrates at aerodynamic Weber numbers $\mathrm{We}_g \gtrsim 12$. To achieve high Weber numbers and to avoid the breakup of the droplets, an apparatus was built including a moving surface. Thus a flywheel of 0.6 m diameter was constructed and on its lateral area, the substrate was mounted hitting the free falling droplets (see Figure 1). In [13] it is emphasised that additional forces due to the rotational movement of the substrate, centrifugal and Coriolis, may be neglected if the droplet diameter is small compared to the distance between the centre of collision and centre of rotation. This was the case during present experiments.

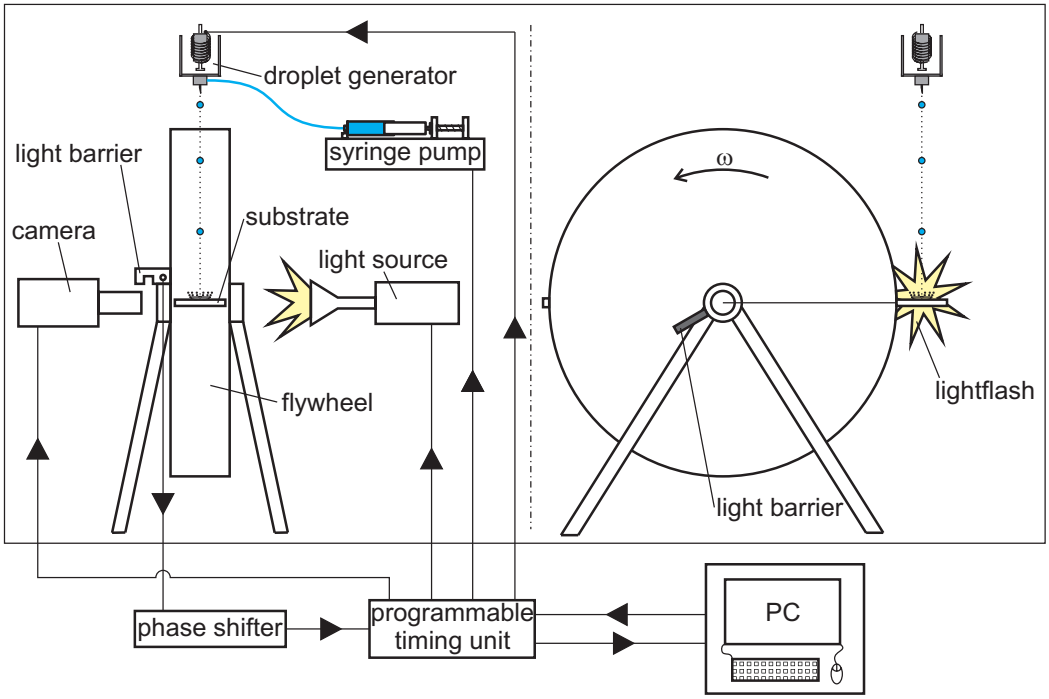

Figure 1. Experimental set up: The flywheel is rotating with constant speed. The impulse of the light barrier is adequately shifted and processed by the programmable timing unit, which itself communicates with the personal computer. Four separate signals control the activity of the droplet generator, the syringe pump, the camera and the light source—a Nd:YAG-Laser with a diffuser optics by LaVision. Phase-locked observation of the impact of single droplets is possible

The apparatus allows the variation of the resulting Weber number by changing the rotational speed ω of the flywheel as well as the variation of the impact angle. Weber numbers up to $\mathrm{We} = 30,000$ can be generated depending on the fluid used and the diameter of the droplets. The resulting Reynolds numbers are small at the same time, because the velocity of the falling droplets is small compared to the rotational speed of the substrate. The examination in hand treats the vertical impact of droplets. Two different Weber numbers were observed. The Table 1 shows the investigated resulting Reynolds numbers Re and the resulting Weber numbers We.

In the current experiments, glass has been chosen as a substrate, but the experimental setup permits easy changing of the substrate material for future investigations. The glass substrate was cleaned with isopropanol and dimethylketone and then made highly wettable by open flame treatment to remove all organic residue. This allows for the reproducible quality of the surface. A secondary effect of the rotational movement was that a fully dry substrate could be provided for every impingement.

The water droplets were generated on demand by a syringe-pump-based droplet generator and fell under the influence of gravity. For the resulting droplets diameter see Table 1, the distribution of the diameter of the primary droplets is shown in Figure 4.

For the shadowgraphy measurements, a double-frame LaVision ImagerPro X camera was used to record the impact from a sideways position. Short back-lighting at uniform high intensity was achieved by a double-pulse Litron Nd:YAG laser. To widen the laser beam and to avoid speckle, a LaVision Diffuser Optics was mounted between the laser and the substrate. Due to the fluorescence of the Diffuser Optics, the duration of the illumination flash was 20 ns.

Table 1. Nominal Weber number $\mathrm{We_{nom}}$, diameter of primary droplets d_D, Sauter diameter d_{32}, falling height H, falling speed v_f, actual Reynolds number Re, rotational speed v_r, and actual Weber number We of the two experiments

$\mathrm{We_{nom}}$	$5,000$	$10,000$
H / m	0.5	0.5
v_f / m/s	2.84 ± 0.03	2.75 ± 0.04
v_r / m/s	8.8	13.8
d_D / 10^{-3}m	2.72 ± 0.04	2.72 ± 0.05
d_{32} / 10^{-3}m	2.72	2.72
Re	500 ± 8	482 ± 9
We	$5,079 \pm 84$	$10,245 \pm 184$

For the research in hand, the size of the field of view was fixed on the base of the two contradicting boundary conditions: Realising the maximum field of view for not loosing the secondary droplets out of sight during the impact and simultaneously obtaining the maximum resolution of the emerging secondary droplets. For this, the actual size of the field of view was chosen to $X \times Y = 25.69{\cdot}10^{-3}$ m $\times$ $38.54{\cdot}10^{-3}$ m at 2672 pixel $\times$ 4008 pixel.

The restriction of the evaluation software is that a particle must have a minimum area of 9 pixel. This means that the smallest secondary droplet being detected has a diameter of $d_{\mathrm{D_{min}}} \approx 33{\cdot}10^{-6}$ m. After all, the item of this paper is to verify that most of the total secondary mass was detected. This enables the evaluation of the total deposited mass as the difference of the primary droplet's mass and the total secondary mass.

The triggering and storage of the photographs was operated by the LaVision software DaVis ParticleMaster. The signal of a light barrier attached to the flywheel was phase shifted and then controlled the chain of impingement, exposure, illumination according to the commands by the software. The time between the release of the droplets and the impingement was adjustable, as well as the moment of illumination itself. By this, phase-locked measurements were realized.

The impingement process at each Weber number was sampled at six release times of the droplets. A higher sampling rate is not useful because the flow field around the rotating flywheel deflects each droplet in a slightly different way, both in sideways direction and in the direction of altitude. This generated rotational flow field and the associated PIV-measurement are not treated in this paper, though. The procedure of the presented evaluation of the secondary mass is not effected by the flow field.

During these measurement series, a number of between 200 and 350 double-frame images were taken. From those the velocity of the primary droplets was evaluated as well as the distribution of the size of primary and secondary droplets. The LaVision software DaVis ParticleMaster software was also used to calculate the primary and secondary droplets' diameter and their position in the images. Those data were then processed with a special code for the evaluation the mass of each detected secondary droplet written in Matlab.

The correct evaluation of the secondary mass calls for a calibration not only of the scale but also of the depth of field the optical setup provides. For the latter the LaVision Calibration Plate was used (see Figure 2). This plate was traversed through the field of view in the direction of the depth at the same adjustment of the focus. Then the pictures were evaluated with that set of parameters giving the best result for the depth-of-field-calibration (DoF-calibration). Afterwards, the same set of parameters was used for the evaluation of the images of the impingement the droplets.

During reconstruction of the secondary mass, the contribution of every detected secondary droplet of every frame within the area of interest is evaluated, following an approach by [16]. It is assumed that all emerging secondary droplets spread in circumferential direction from the centre of impact equally during the vertical impact. Thus, the contribution of each single detected secondary droplet j to the entire secondary mass in the image I is

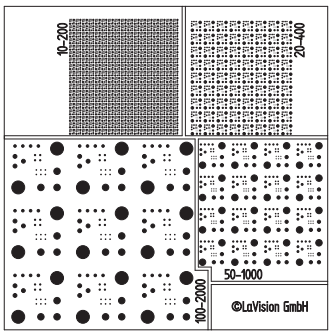

Figure 2. The calibration plate for calibration and validation of ParticleMaster shadowgraphy systems (source: LaVision GmbH)

estimated to be

$$m_I = \frac{2\pi}{\delta} x_j \, m_j \; . \tag{2}$$

It is δ the depth of field, x_j the position of the droplet j in radial direction and m_j is its mass. Figure 3 shows the area of interest and its geometry.

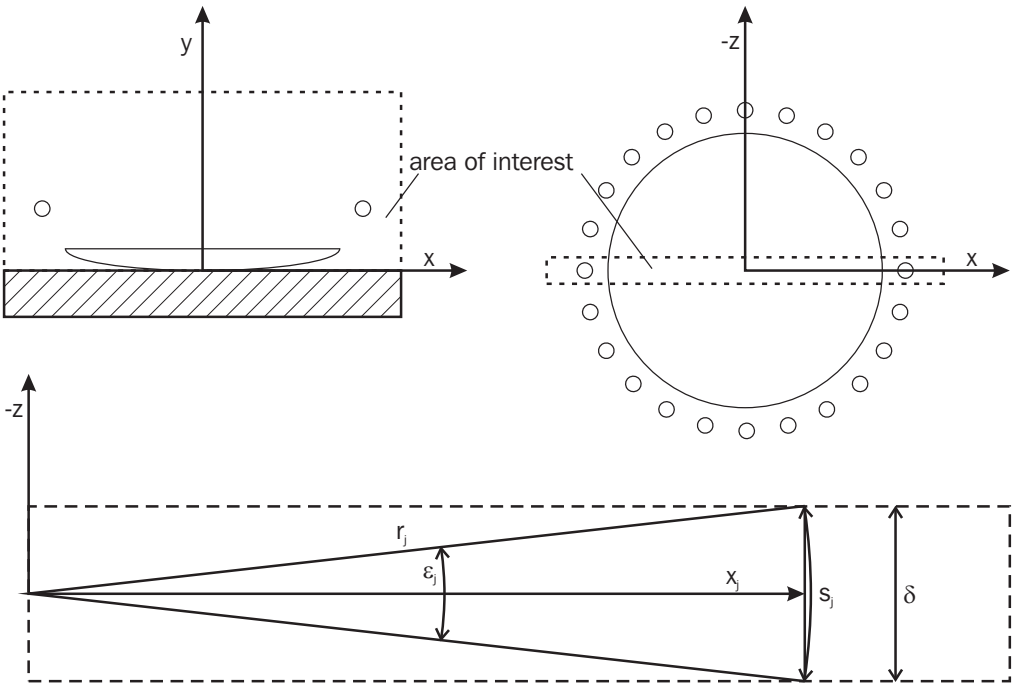

Figure 3. The area of interest in detail. Upper left: View of the camera; upper right: Area of interest from the top; lower: Details of the area of interest and its geometry.

Hence, the knowledge of the depth of field of the used optical setup is essential for calculating the overall secondary mass. According to [17], the depth of field depends on the size of the object observed. For this, the DoF-calibration is used as mentioned above. The resulting ratio of the depth of field δ to the diameter d of a detected droplet in the experiments was $\delta/d = 8.24$. This information allows for the calculation of the individual depth of field of each single detected secondary droplet, named δ_j. Further more, the present images give information about either side of the centre of impact. Thus the summation of a single detected secondary droplet only covers the angle $[0 \ldots \pi]$. Accordingly, the contribution m_I of one single image I containing n_I detected secondary droplets

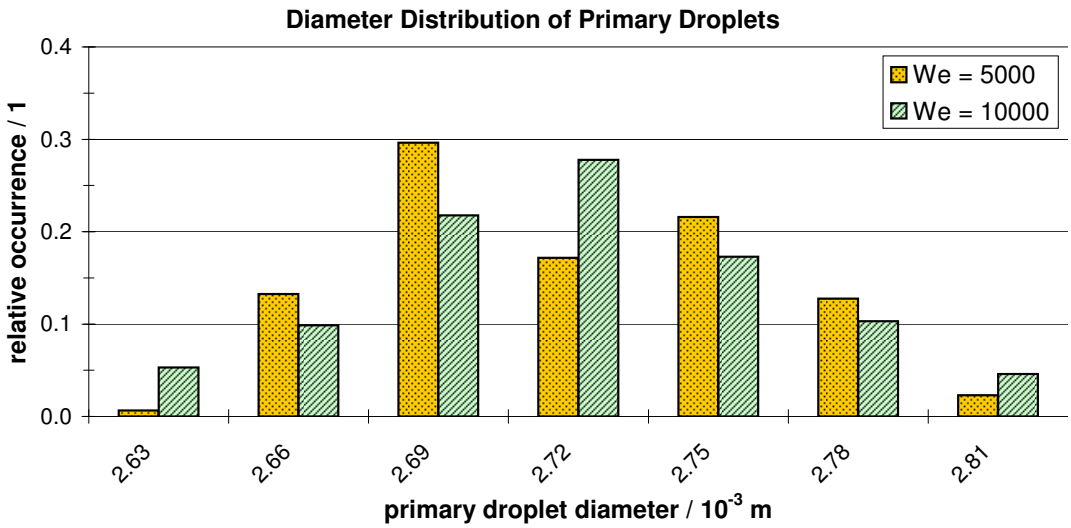

Figure 4. Distribution of the diameter of the primary droplets for the four Weber Numbers We $= 5,000$ and We $= 10,000$. The given numbers denote the centre of each diameter class.

reads

$$m_I = \pi \sum_{j=1}^{n_I} \frac{x_j}{\delta_j} m_j \ . \tag{3}$$

In [16] it is argued that for a given depth of field a certain radial position must not be fallen below to reach an acceptable measure of accuracy by the simplification adopted in (2) and (3), respectively. For the evaluation in hand, a difference between the arc length s (see Figure 3 bottom) and the depth of field δ of 5% is accepted for a valid evaluation of the data. This yields $0.05 \leq 1 - \cos(\varepsilon/2)$ and $\varepsilon_{\text{max}} = 36.4°$, respectively. Accordingly, the maximum of ratio of the depth of field to the radial position of a secondary droplet is

$$\frac{\delta_j}{x_j} = 2 \tan\left(\varepsilon_{\text{max}}/2\right) = 0.66 \ . \tag{4}$$

Based on this, one estimates the resulting uncertainty Δ of the position of the droplet within the depth of field as its exact depth-position z_j is not known:

$$\Delta = 1 - 2\frac{x_j}{\delta_j} \arctan\left(\frac{z_j}{2\,x_j}\right) \ . \tag{5}$$

The greatest uncertainty is obtained if $z_j = \delta_j$. Inserting this and the minimal accepted x_j to (5), in the worst case, Δ becomes $\Delta = 0.034$. The maximal uncertainty is calculated for each detected secondary droplet and the mean value amounts in all cases less than 1%. This evaluation error is small compared to the error imposed by the scatter of the centre of impact. This causes a certain loss of secondary droplets disappearing outside of the area of interest. The magnitude of this error is discussed at the end of the next section.

Results and Discussion

For the evaluation of the primary droplets, between 50 and 75 valid images exist for every release time of the primary droplet. In Figure 4, the distribution of primary droplet diameter is given. The droplets can be generated with a variation of about 1.5%, while the distribution is not the same in both measurement series. The main influence on this disparity preasumbly is again the flow field around the flywheel. The flow field induces oscillation and deformation to the droplets resulting in the difference in the detected diameters. During the evaluation, the limit of the accepted deformation is a centricity of 80%, while a perfect circle has a centricity of 100%. Increasing the limit whould reshape the distribution of primary droplet diameter slightly, but the accuracy of about 1.5% of the droplets generated is acceptable.

For the measurements at Weber number We $= 5,000$, corona splashing was observed. This agrees with the results of [14] for the impingement of water droplets on a glass surface. Otherwise, at We $= 10,000$, most of the

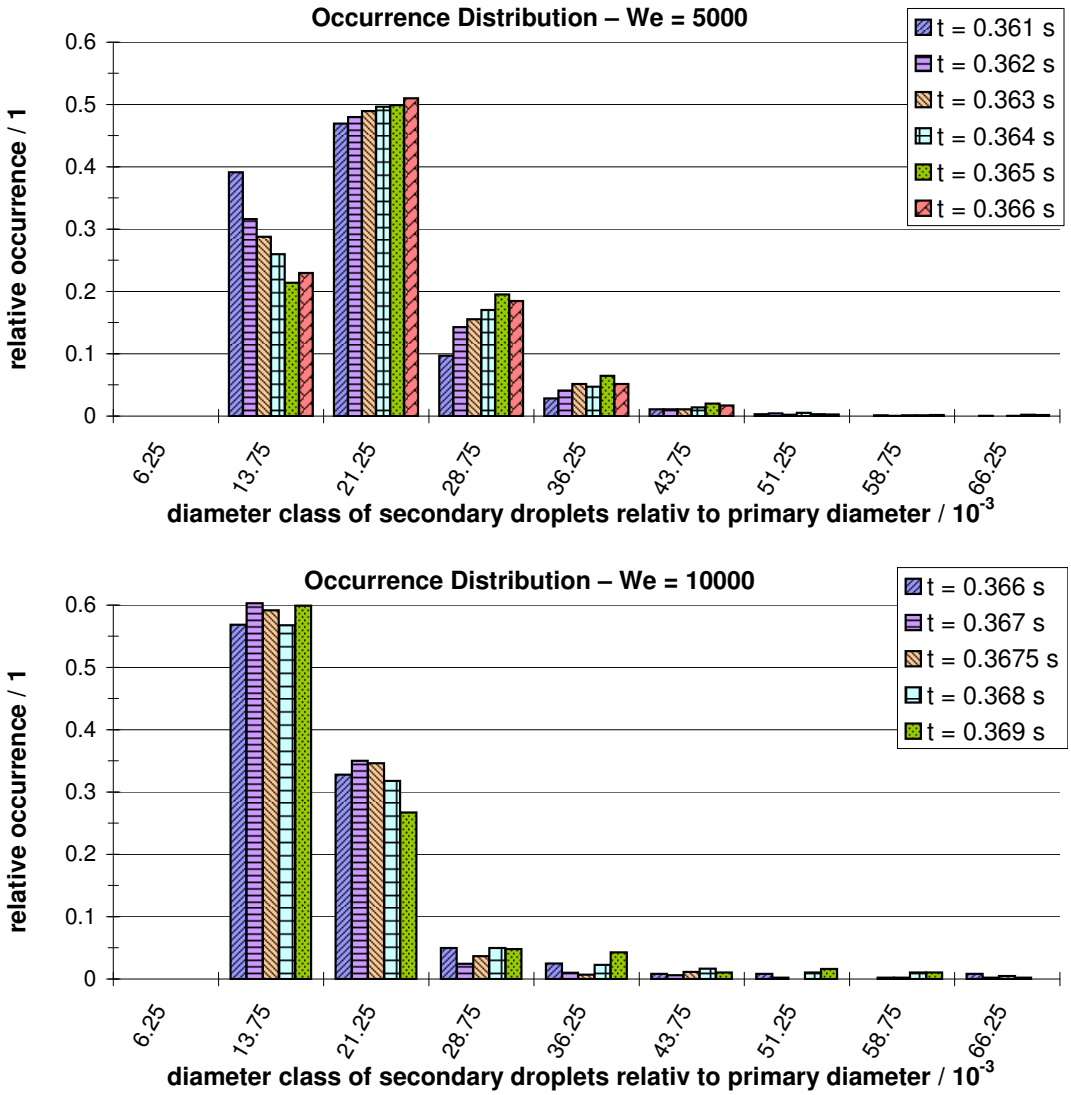

Figure 5. Distribution of the relative occurrence of secondary droplet's size relative to the primary diameter at time t after the release of primary droplet—above We $= 5,000$, below We $= 10,000$. The given numbers denote the centre of each diameter class.

impinging droplets show the corona splashing as well. This does not match the findings of [14], where prompt splashing was observed at We $= 7,354$. The delayed onset of prompt splashing in the experiments in hand could be linked to the different wettability of the surface. In [14] it is not told, if the surface was cleaned in any way.

The number of valid images allowing the evaluation of secondary droplets lies between 50 and 100 per release time. The evaluation of each single release time is valid, if the number of detected secondary droplets is at least 100 in total. Normally this number is greater than 250. Only in the early stages of the impact, it is less than this. The Figure 5 shows the histogram of the emerging secondary droplet diameters. For the measurements at We $= 10,000$, there are only five of the six release times shown, because at $t = 0.365$ s, in the greater part the impingement did not take place, yet. Note that for each class the mid value of the class is given, and remember that the smallest detectable droplet has a size of $d_{\mathrm{D_{min}}} \approx 33{\cdot}10^{-6}$ m. For the mean diameter of the primary droplets of $\bar{d}_{\mathrm{D}} = 2.72{\cdot}10^{-3}$ m this results in the minimal resolvable ratio of the secondary droplet size to the primary diameter of $d_{\mathrm{D_{min,sec}}}/\bar{d}_{\mathrm{D}} \approx 12 \cdot 10^{-3}$.

Further, the occurrence distribution at We $= 5,000$ shows a reduction of the smallest droplets during the impact process, while larger secondary droplet become more often. Different mechanisms to create secondary droplets of different sizes like proposed in [8] could reason this result, even if in [8] the impingement on a thin film was reported. Thus, a similar process can be expected ([4]).

Another explanation can be found in the remaining kinetic energy after the impact. In the first phase of the

impingement parts of the kinetic energy of the drop impact dissipates by the viscous forces and parts of it convert into surface energy associated with the highly increased free-surface area ([7]) of the lamella. The remaining kinetic energy feeds the formation of secondary droplets. The less the remaining energy is the greater and slower the emerging secondary droplets become, until the residual top of impacting drop is expended.

Looking at the the occurrence distribution at We $= 10,000$, the number of the smallest droplets is increased clearly. In contrast to the distribution at We $= 5,000$, the fraction of the smallest droplets does not diminish during the impact process. The distribution shows a similar characteristics for all release times at We $= 10,000$. The higher kinetic energy seems to enable the generation of a higher quota of small secondary droplets. Unfortunately the velocity of the secondary droplet could not be determined during the measurements. The investigation of even higher Weber numbers will deliver more information.

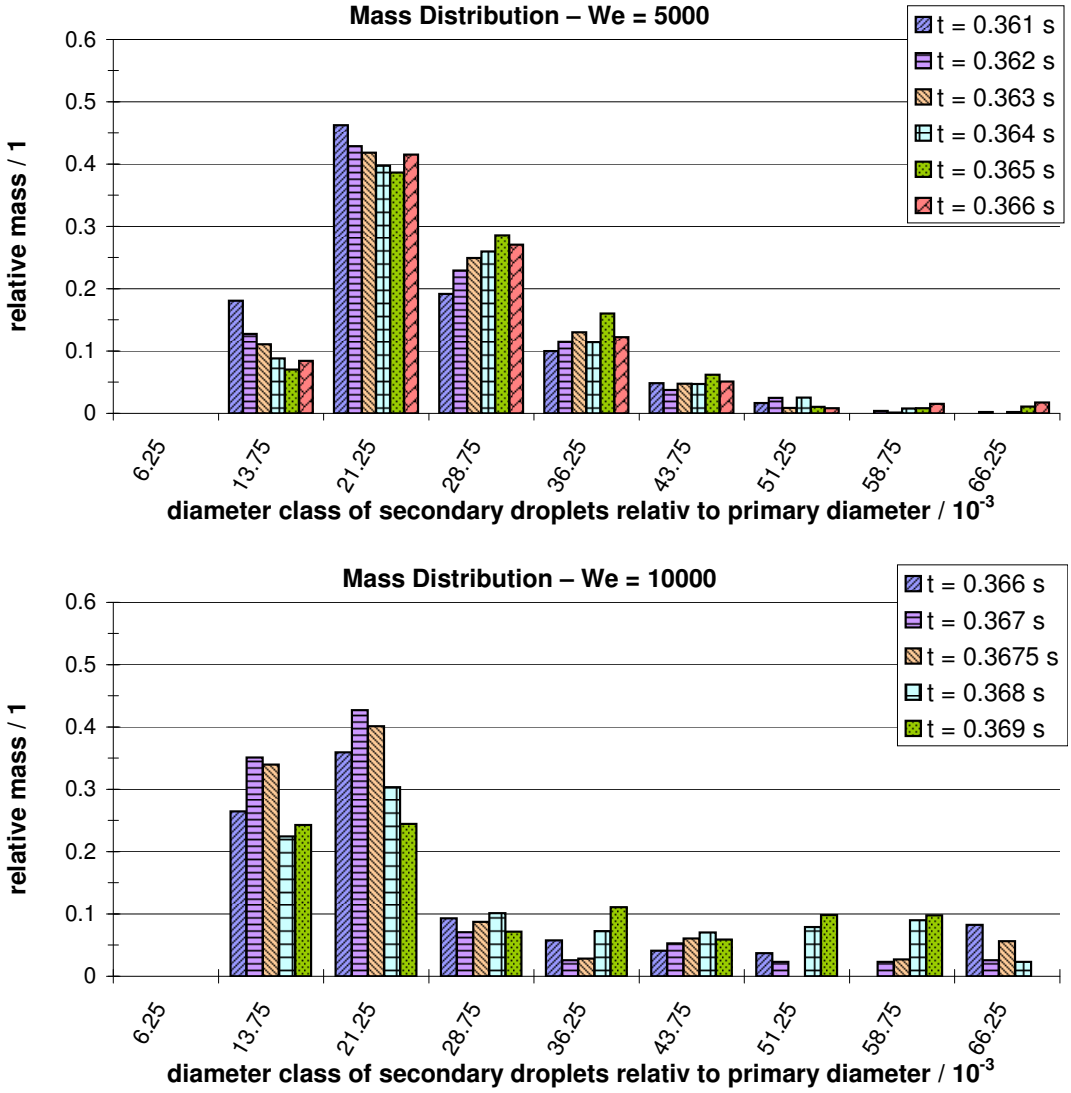

Figure 6. Distribution of the relative mass of secondary droplet's size relative to the primary diameter at time t after the release of primary droplet—above We $= 5,000$, below We $= 10,000$. The given numbers denote the centre of each diameter class.

As the interest of this examination is whether the total deposited mass can be detected by the optical technique used, it is important how much of the secondary mass is implied in each class of secondary droplets. The Figure 6 shows the distribution of the relative mass to the different classes. At We $= 5,000$ the diameter classes of $d_{\mathrm{D_{sec}}}/d_{\mathrm{D_{prim}}} = 21.25 \cdot 10^{-3}$ and above largely contain more than 80% of the detected mass. In this case one can assume that the mass contained by droplet classes below $d_{\mathrm{D_{sec}}}/d_{\mathrm{D_{prim}}} = 13.75 \cdot 10^{-3}$ can be neglected for the evaluation of the total deposited mass. At We $= 10,000$, the distribution is not as distinct, but looking at the

envelope of the histogram, the maximum of relative mass lies in the class of $d_{\mathrm{D_{sec}}}/d_{\mathrm{D_{prim}}} = 21.25 \cdot 10^{-3}$. Extending the envelope to classes of smaller droplets again delivers a negligible quota of mass in the classes not resolved.

The main sources of measuring inaccuracy are the variation of the centre of impingement and of the detected droplet diameter due to the rotational flow field around the flywheel, the uncertainty of the correct position of detected droplet in the direction of the depth of field and the error concerning the resolution of the secondary mass. The scatter of the centre of impact causes the inaccuracy of about 30%, because secondary droplets get lost outside of the area of interest. This error is estimated by shifting the distribution of the secondary droplets along the x-axis by the value of the standard deviation of the centre of impact. The variation of the detected droplet diameter produces a inaccuracy of about 1.5%. The uncertainty of the correct position of a droplet in the direction of the depth of field is less than 1.0%. Finally, the measuring error concerning the resolution of the secondary mass amounts to approximate 10%. Hence, the total inaccuracy lies in the range of 32%.

Conclusions

It was shown, that the present measurements with optical method do resolve the greater part of the emerging secondary mass during the impact of single droplets on smooth dry surfaces at Weber numbers of We $= 5,000$ and We $= 10,000$. Though the minimal detectable diameter of droplets is limited to sizes with significant relative occurrence, the contribution of those droplets to the total secondary mass is negligible. Extending the envelope of the mass distribution to classes of droplet beyond the resolution capability yields an mass quota of approximate 10% to the total mass not beeing dissolved.

The evaluation has shown as well that there is work to do to increase the accuracy of the measurements. The main problem is the scatter of the centre of impact causing the diminution of detectable secondary droplets. As the extension of the area of interest would decrease the optical resolution, using a shielding tube (see [4, 5]) would be an adequate means. By this, the measurement error could presumably be decreased to less than 20%.

In the next step, the secondary mass at every release time of the primary droplet will be summed up to one cumulative magnitude, the total deposited mass. This will be done by a weighting factor, wich is the ratio of the time step between two different release times and the time within wich all droplets in the area of interest has been replaced by new secondary droplets. This weighting factor depends on the number of different release times the hole impingement process was sampled with. Thus, it can be less than, equal to or greater than 1. Further more the weighting factor is a function of the dimensions of the area of interest and the mean velocity of the secondary droplets. Further more, Weber numbers up to We $= 30,000$ will be treated soon.

References

[1] Worthington, A.M., *A Study of Splashes*, Longmans, Green & Co., 1908.

[2] Marengo, M., Rioboo, R., Sikalo, S., Tropea, C., *Fourteenth International Conference on Liquid Atomization and Spray Systems*, Manchester, UK, July 1998, pp. 114–121.

[3] Yarin, A.L. and Weiss, D.A., *Journal of Fluid Mechanics* 283:141–173 (1995).

[4] Rioboo, R., Tropea, C., Marengo, M., *Atomization and Sprays* 11:155–166 (2001).

[5] Rioboo, R., Marengo, M., Tropea, C., *Experiments in Fluids* 33:112–124 (2002).

[6] Rein, M., *Fluid Dynamics Research* 12:61–93 (1993).

[7] Yarin, A.L., *Annual Review of Fluid Mechanics* 38:159–192 (2006).

[8] Range, K. and Feuillebois, F., *Journal of Colloid and Interface Science* 203:16–30 (1998).

[9] Kuthada, T., Widdecke, N., Wiedemann, J., *4th MIRA International Vehicle Aerodynamics Conference*, Warwick, UK, October 2002.

[10] Bannister, M., *SAE 2000 World Congress*, Detroit, Michigan, USA, March 2000, pp. 97–113.

[11] Szilder K., Mcilwain S., Lozowski, E., *ICAS 2006, 25th Congress of the International Council of the Aeronautical Science*, Hamburg, Germany, September 2006, pp. 2.5.1–2.5.8.

[12] Mehdizadeh, N.Z., Chandra, S., Mostaghimi, J., *ASME Heat Transfer Division*, Orlando, Florida, USA, November 2000, pp. 397–405.

[13] Mehdizadeh, N.Z., Chandra, S., Mostaghimi, J., *Journal of Fluid Mechanics* 510:353–373 (2004).

[14] Pan, K.-L.; Tseng, K.-C.; Wang, C.-H. *Experiments in Fluids* 48:143–156 (2010).

[15] Armster, S.Q., Delplanque, J.-P., Rein, M., Lavernia, E.J., *International Materials Reviews* 47:265–301 (2002).

[16] Weiss, D.A., "Periodischer Aufprall monodisperser Tropfen gleicher Geschwindigkeit auf feste Oberflächen", Mitteilungen aus dem Max-Planck-Institut für Strömungsforschung No. 112 (1993).

[17] Kim, K.S. and Kim, S.S., *Atomization and Sprays* 4:65–78 (1994).